Global neutrino data and recent reactor fluxes: status of three-flavour oscillation parameters

Thomas Schwetz†, Mariam Tórtola§ and J. W. F. Valle§

† Max-Planck-Institut für Kernphysik, PO Box 103980, 69029 Heidelberg, Germany
§ AHEP Group, Instituto de Física Corpuscular – C.S.I.C./Universitat de València, Edificio Institutos de Paterna, Apt 22085, E–46071 Valencia, Spain

E-mail: schwetz@mpi-hd.mpg.de, mariam@ific.uv.es, valle@ific.uv.es

Abstract. We present the results of a global neutrino oscillation data analysis within the three-flavour framework. We include latest results from the MINOS long-baseline experiment (including electron neutrino appearance as well as anti-neutrino data), updating all relevant solar (SK II+III), atmospheric (SK I+II+III) and reactor (KamLAND) data. Furthermore, we include a recent re-calculation of the anti-neutrino fluxes emitted from nuclear reactors. These results have important consequences for the analysis of reactor experiments and in particular for the status of the mixing angle θ_{13}. In our recommended default analysis we find from the global fit that the hint for non-zero θ_{13} remains weak, at 1.8σ for both neutrino mass hierarchy schemes. However, we discuss in detail the dependence of these results on assumptions concerning the reactor neutrino analysis.

keywords: Neutrino mass and mixing; neutrino oscillation; solar and atmospheric neutrinos; reactor and accelerator neutrinos

1. Introduction

The discovery of neutrino mixing and oscillations provides firm evidence for physics beyond Standard Model, opening a new era in particle physics. Here we update the three-neutrino oscillation results of Ref. [1] ‡ with a special emphasis on the new reactor anti-neutrino flux results of Refs. [5, 6] which have an important impact on the determination of the mixing angle θ_{13}. We include new data from the MINOS Collaboration, both for $\nu_\mu \to \nu_e$ transitions [7] and ν_μ disappearance [8, 9], the latest Super–Kamiokande (SK) solar [10, 11] and atmospheric [12] neutrino data, as well as recent KamLAND reactor data [13]. Our goal is to summarize the results of the three-flavour neutrino oscillation analysis paying attention to sub-leading three-flavor effects where they are most relevant, as well as to the effects of the new anti-neutrino flux

‡ When referring to this paper we include also its updates available at arXiv:0808.2016v3 [hep-ph]. Further technical details of the analysis as well as earlier experimental references are also given in our previous review in [2]. For other global analyses see [3, 4].

emitted from nuclear reactors which has been re-evaluated in Ref. [5]. The reported value of the $\bar{\nu}_e$ flux is about 3% higher than from previous calculations. This has important consequences for the interpretation of data from reactor experiments. We discuss the implications of the new reactor neutrino flux for the determinations of oscillation parameters, in particular its effect on the mixing angle θ_{13}. We find that due to the new fluxes the results depend on the inclusion of short-baseline reactor data from distances $\lesssim 100$ m.

In Sec. 2 we present the updated analysis in the "atmospheric sector", discussing the Super Kamiokande I+II+III data [12] in Sec 2.1 and the MINOS disappearance results taking into account the solar squared-mass splitting and discussing the slight tension between neutrino and anti-neutrino data in Sec. 2.2. In Sec. 2.3 we focus on the combined SK+MINOS analysis and the determination of θ_{13} from these data. Sec. 3 contains the discussion of the reactor neutrino data in the light of the new predicted anti-neutrino fluxes, and in Sec. 4 we discuss solar neutrino data as well as KamLAND and the other reactor experiments. The results of the global fit are summarized in Sec. 5 including a detailed discussion of the status of θ_{13}. In particular we discuss the dependence of the θ_{13} determination upon assumptions concerning the reactor anti-neutrino data analysis. Conclusions follow in Sec. 6.

2. The atmospheric sector – SK I+II+III and MINOS

2.1. Super-Kamiokande I+II+III data

We include in our analysis the full sample of atmospheric neutrino data from all three phases of the Super-Kamiokande experiment [12], using directly the χ^2 map provided by the Super-Kamiokande collaboration. The atmospheric neutrino oscillation analysis is performed within the one mass scale approximation, neglecting the effect of the solar mass splitting, as in our previous papers [1, 2] §.

In Fig. 1 we show the results of our previous atmospheric neutrino analysis from Refs. [1, 2] including data from the first phase of the Super-Kamiokande experiment, compared to the new analysis included in this update, based on the Super-Kamiokande data from all three phases of the experiment. The differences between the two analyzes are clearly noticeable, with an improved determination of both oscillation parameters. As we will see in the following, once data from neutrino disappearance at the MINOS long-baseline experiments are included in the analysis, the improvement in the determination of Δm^2_{31} due to the recent atmospheric neutrino data is "hidden" by the more constraining restrictions imposed by long-baseline data. Nevertheless, this new atmospheric analysis will be important when constraining the mixing angle θ_{23} and also θ_{13}.

§ Preliminary results towards a full 3-flavour atmospheric neutrino analysis have been presented in [14], we look forward to the corresponding information becoming publicly available.

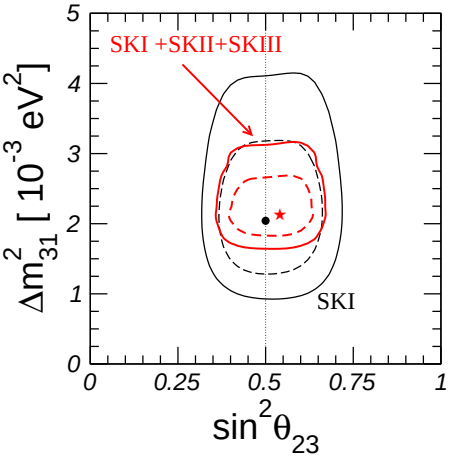

Figure 1. Comparison of our previous SK-I atmospheric analysis (in black) and the new analysis using the latest atmospheric data from SK-I, SK-II, SK-II (in red) for inverted mass hierarchy. Best fit points denoted by a dot or star follow the same colour code.

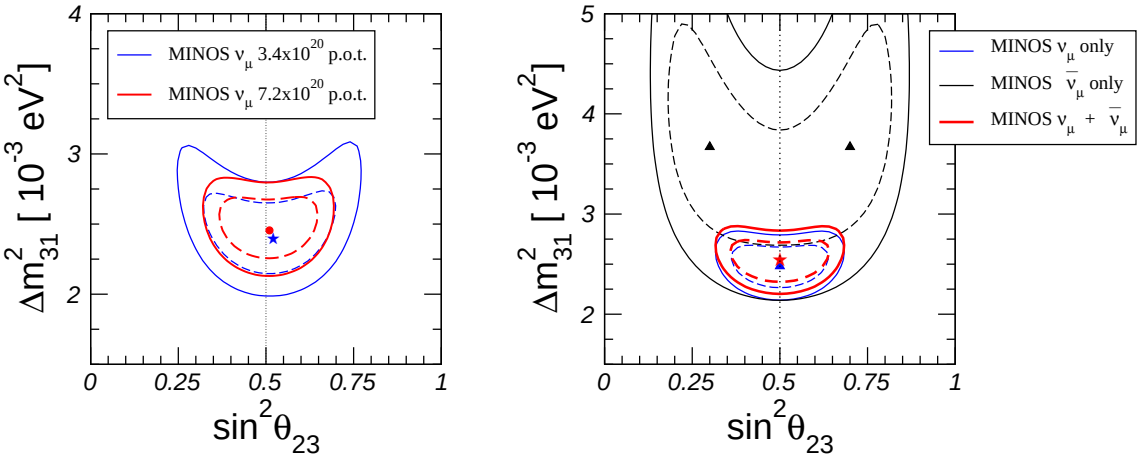

Figure 2. Determination of atmospheric neutrino parameters by the MINOS long-baseline experiment. Left panel: previous (3.36×10^{20} p.o.t.) versus current ($7.2{\times}10^{20}$ p.o.t.) ν_μ data. Right panel: allowed regions from recent MINOS ($7.2{\times}10^{20}$ p.o.t.) data, using neutrinos-only, anti-neutrinos-only, and the combination. Both panels assume normal hierarchy. As before, best fit points follow the same colour code.

2.2. MINOS disappearance data

At the Neutrino 2010 Conference, the MINOS Collaboration has presented new data from their searches of ν_μ disappearance, both from the neutrino ($7.2{\times}10^{20}$ p.o.t.) and the anti-neutrino ($1.71{\times}10^{20}$ p.o.t) running mode [8]. We perform a re-analysis of the data from [8] within a full three-flavour framework using the GLoBES software [15] to simulate the experiment. In addition to matter effects, we include also the effect of Δm^2_{21} as well as θ_{13} and the CP-phase δ in the analysis of the disappearance and appearance channels. Since in our analysis MINOS data are the only ones sensitive to the phase δ we always minimize the MINOS χ^2 with respect to δ.

In Fig. 2 we compare the analysis of new MINOS data with the previous data release (left panel). Apart from the smaller size of the allowed regions due to the increase in statistics, we notice also a change in the shape of the regions. This follows from the inclusion of the sub-leading three-flavour effects included in this new analysis.

In the right panel we illustrate the impact of the (still small) anti-neutrino sample. From the figure one can see that there is a slight tension between the neutrino and anti-neutrino results: there is no overlap of the allowed regions at less than 90% CL. However, at 3σ the results of both are fully consistent. We find the following χ^2 minima and goodness-of-fit (GOF) values:

$$\begin{aligned} \nu: &\quad \chi^2_{\mathrm{min},\nu} = 24.4/(27-2) \quad \mathrm{GOF} = 49.6\% \\ \bar{\nu}: &\quad \chi^2_{\mathrm{min},\bar{\nu}} = 15.0/(13-2) \quad \mathrm{GOF} = 18.4\% \\ \nu+\bar{\nu}: &\quad \chi^2_{\mathrm{min,tot}} = 46.1/(40-2) \quad \mathrm{GOF} = 17.3\% \end{aligned} \tag{1}$$

Hence the combined neutrino and anti-neutrino fit provides still an acceptable GOF. Using the consistency test from Ref. [16] yields $\chi^2_{\mathrm{PG}} = \chi^2_{\mathrm{min,tot}} - \chi^2_{\mathrm{min},\nu} - \chi^2_{\mathrm{min},\bar{\nu}} = 6.6$. The value of χ^2_{PG} must be evaluated for 2 degrees of freedom, which implies that neutrino and anti-neutrino data are consistent with a probability of 3.7%. This number indicates a slight tension between the sets, at the level of about 2.1σ. In the following we will use only neutrino data in the global analysis. It is clear from Fig. 2 (right) that adding also anti-neutrino data would have negligible impact on the global result.

2.3. The atmospheric sector: combined MINOS + atmospheric analysis and θ_{13}

Combining the new atmospheric and MINOS disappearance data we obtain new global constraints on the atmospheric neutrino oscillation parameters. The results are shown in Fig. 3. As before, Δm^2_{31} is determined mainly by the MINOS data, while the atmospheric data are more important in determining the mixing parameter $\sin^2\theta_{23}$. Notice that the sub-leading effects of Δm^2_{21} lead to different best fit points for $|\Delta m^2_{31}|$, that depend on whether the mass hierarchy is normal (NH) or inverted (IH). We find the following best fit values with errors at 1σ:

$$|\Delta m^2_{31}| = \begin{cases} 2.45 \pm 0.09 & \times 10^{-3}\,\mathrm{eV}^2 \qquad (\mathrm{NH}) \\ 2.34^{+0.10}_{-0.09} & \times 10^{-3}\,\mathrm{eV}^2 \qquad (\mathrm{IH}) \end{cases} \tag{2}$$

The corresponding allowed regions are shown in Fig. 3 (right). The reason for this apparent shift is just a result of our parameterization, using Δm^2_{31} for both hierarchies, and changing only the sign of it to distinguish them. Hence, in NH the "largest" frequency is given by $|\Delta m^2_{31}|$, while in IH it is $|\Delta m^2_{31}| + \Delta m^2_{21}$, which explains why $|\Delta m^2_{31}|$ is smaller for IH. Eq. 2 shows that these sub-leading effects must be included given the present accuracy, since they are at the level of the 1σ error on Δm^2_{31}.

Now we move to appearance MINOS data. The MINOS Collaboration has recently also reported new data from the search of $\nu_\mu \to \nu_e$ transitions in the Fermilab NuMI beam [7]. The new data are based on a total exposure of $7{\times}10^{20}$ protons-on-target, more than twice the size of the previous data release [17]. The new MINOS far detector

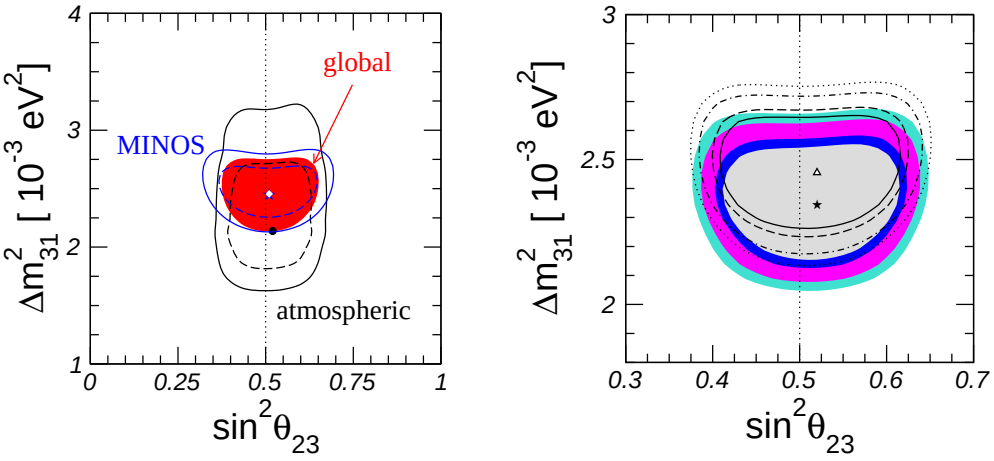

Figure 3. Determination of the atmospheric oscillation parameters. Left: interplay of atmospheric (black) and MINOS disappearance (blue) data and the combination (red/shaded region) for normal hierarchy at 90% CL (dashed) and 3σ (solid). Right: combined allowed regions for normal (black curves) and inverted hierarchy (colored regions) at 90%, 95%, 99%, 99.73% CL.

data consists of 54 electron neutrino events, while, according to the measurements in the MINOS Near Detector, $49.1 \pm 7.0(stat) \pm 2.7(syst)$ background events were expected. Hence the observed number of events is in agreement with background expectations within 0.7σ and the hint for a non-zero value of θ_{13} present in previous data [17] has largely disappeared. In fact, we see that once we include the new MINOS data in our analysis, a smaller best fit point of θ_{13} is obtained and, as a result, the hint for θ_{13} is less significant than before: for both hierarchies we find only a 0.8σ hint when using new MINOS data versus 1.3σ obtained with the previous MINOS appearance data, see e.g. [18] for a discussion.

Atmospheric neutrino data from Super-Kamiokande I+II+III described in the previous section implies a best fit point very close to $\theta_{13} = 0$ [12], with $\Delta\chi = 0.0(0.3)$ for $\theta_{13} = 0$ for NH (IH). However, in the combination with MINOS disappearance and appearance data we even find a slight preference for $\theta_{13} > 0$, with $\Delta\chi^2 = 1.6(1.9)$ at $\theta_{13} = 0$ for NH (IH). As shown in Fig. 4 this happens due to a small mismatch of the best fit values for $|\Delta m^3_{31}|$ at $\theta_{13} = 0$, which can be resolved by allowing for non-zero values of θ_{13} [3]. This is similar to the hint for $\theta_{13} > 0$ coming from a slight tension between solar and KamLAND data, see Ref. [1]. Therefore, the hint for $\theta_{13} > 0$ from atmospheric + LBL data becomes slightly stronger compared to the previous data.

3. New reactor fluxes and implications for oscillation parameters

Up to very recently the interpretation of neutrino oscillation searches at nuclear power plants was based on the calculations of the reactor $\bar{\nu}_e$ flux from Ref. [19]. Indeed, the observed rates at all reactor experiments performed so-far at distances $L \lesssim 1$ km are consistent with these fluxes, therefore setting limits on $\bar{\nu}_e$ disappearance. Recently the

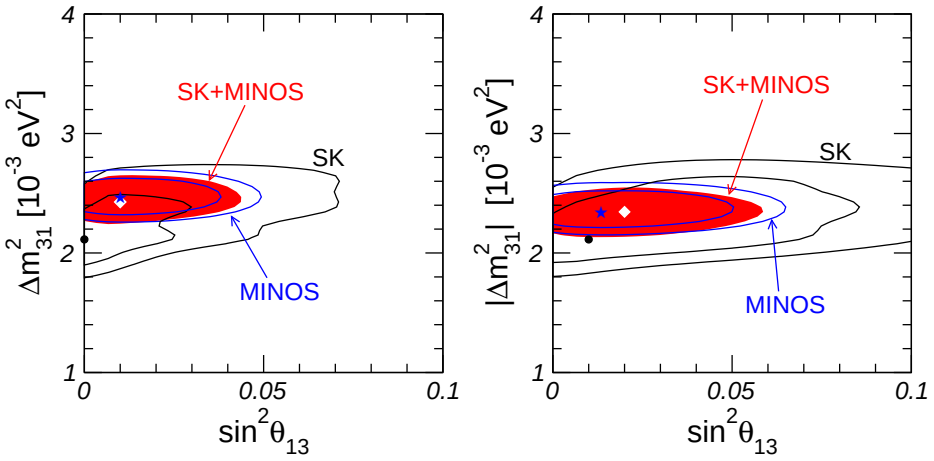

Figure 4. Allowed regions at 1σ and 90% CL for atmospheric (SK) and MINOS disappearance and appearance data in the plane of $\sin^2\theta_{13}$ and Δm^2_{31} for NH (left) and IH (right). Combined data is shown as shaded/red region at 90% CL. The black dot, blue star, white diamond correspond to the best fit points of SK, MINOS, SK+MINOS, respectively.

flux of $\bar{\nu}_e$ emitted from nuclear power plants has been re-evaluated [5], yielding roughly 3% higher neutrino fluxes than assumed previously. As discussed in Ref. [6] this might indicate an anomaly in reactor experiments at $L \lesssim 1$ km, which according to the new fluxes observe a slight deficit. For the Chooz and Palo Verde experiments at $L \simeq 1$ km a non-zero θ_{13} could lead to $\bar{\nu}_e$ disappearance accounting for the reduction of the rate. However, Δm^2_{13} and θ_{13} driven oscillations will have no effect in short-baseline (SBL) experiments with $L \lesssim 100$ m.

Motivated by this situation we include here also the SBL reactor experiments Bugey4 [21], ROVNO [22], Bugey3 [23], Krasnoyarsk [24], ILL [25], and Gösgen [26] via the rate measurements summarized in Table II of [6], in addition to the fit of the KamLAND, Chooz [27] and Palo Verde [28] experiments. We use the neutrino fluxes from the isotopes ^{235}U, ^{239}Pu, ^{238}U, ^{241}Pu obtained in [5]. For each reactor experiment we take into account the appropriate relative contribution of the isotopes to the total flux and we include the uncertainty on the integrated flux for each isotope given in Table I of [6], correlated among all experiments. The total error on fluxes from ^{235}U, ^{239}Pu, ^{241}Pu are at the level of 2%, where we assume that an error of 1.8% is fully correlated among the three isotopes, due to a common normalization uncertainty of the corresponding beta-spectra measured in [19].

The SBL reactor data is summarized in Fig. 5. We show the observed rate relative to the predicted rate based on old and new flux calculations. Due to the slightly higher fluxes according to [5] all experiments observe a smaller ratio with the new fluxes. In Fig. 5 we show also the result of a fit to the data with the predicted fluxes, allowing the four neutrino fluxes to float in the fit subject to the uncertainties as described above. In the fit we assume that the experimental systematic errors of the three data points from Bugey3, Gösgen, and Krasnoyarsk, as well as Bugey4 and ROVNO are correlated, due

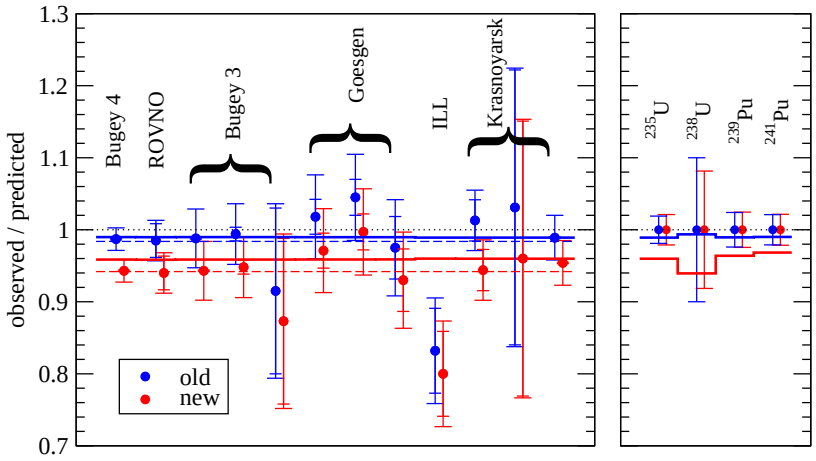

Figure 5. Short-baseline reactor data. We show the observed rate relative to the predicted rate based on old [19] (blue) and new [5, 6] (red) flux calculations. Small error bars show statistical and uncorrelated systematic uncertainties, large error bars include in addition correlated systematic Al uncertainties. The solid histograms correspond to the fitted prediction shifted due to the uncertainty on the fluxes [6], as indicated in the right panel. The dashed lines show the best fit assuming a free overall normalization of reactor fluxes. See text for details.

to the same experimental technique. We obtain $\chi^2 = 8.1(13.0)$ for 12 degrees of freedom using old (new) fluxes. Clearly old fluxes provide a better fit to the data, whereas the χ^2 for new fluxes is still acceptable (P-value of 37%). Such a good fit can be obtained by a rescaling of the fluxes (subject to the quoted uncertainties) as shown in the right panel.

The dashed lines in the figure correspond to a fit where we introduce an overall factor f in front of the fluxes, which we let float freely in the fit. For the old fluxes we find the best fit value of $f = 0.984$ with $f = 1$ within the 1σ range. In contrast, for new fluxes we obtain $f = 0.942 \pm 0.024$, and $f = 1$ disfavored with $\Delta\chi^2 = 6.2$ which corresponds to about 2.5σ. This is the origin of the "reactor anti-neutrino anomaly" discussed in [6]. A possible explanation of this anomaly could be the presence of a sterile neutrino "visible" in this oscillation channel but not in the solar and/or atmospheric conversions, the so-called 3+1 scenario, see e.g. [29]. However, within the uncertainties on the neutrino flux prediction, the goodness of fit of the new fluxes to SBL reactor data is still rather good. Given this somewhat ambiguous situation, in the following we will present results for 3-flavour oscillations adopting different assumptions on reactor neutrino fluxes: (a) motivated by the excellent goodness of fit of SBL data to the new flux prediction we take fluxes and the quoted uncertainties at face value, and (b) we introduce the free flux normalization f in the fit. This second option takes into account the possible presence of a sterile neutrino or some other correlated effect on all reactor neutrino fluxes. In this scenario the SBL reactor experiments effectively serve as near detectors determining the flux which is then used as input for the oscillation analysis at longer baselines.

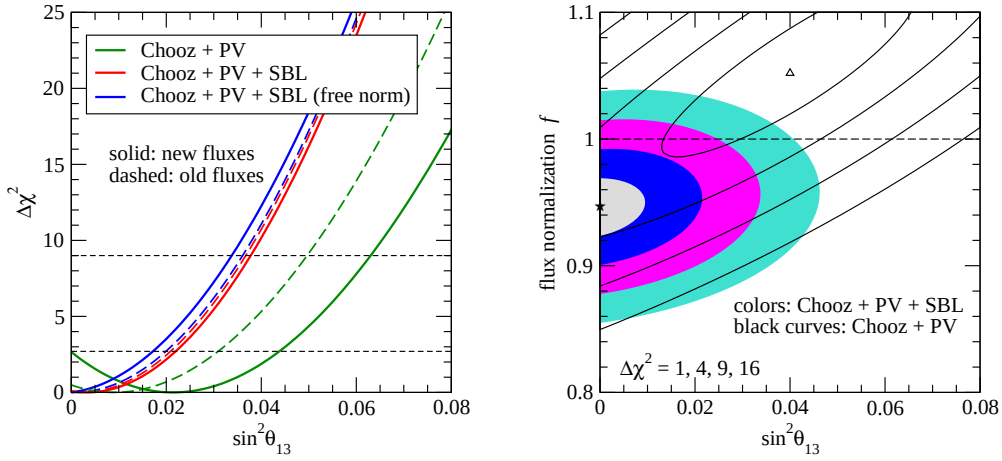

Figure 6. Left: $\Delta\chi^2$ as a function of $\sin^2\theta_{13}$ for the Chooz and Palo Verde (PV) reactor experiments (green), and in combination with the short-baseline (SBL) experiments from Fig. 5. Solid (dashed) curves refer to the new (old) reactor anti-neutrino fluxes. For the blue curves ("free norm") a free overall normalization factor has been introduced for the reactor fluxes. In this figure we fix $\Delta m^2_{31} = 2.45\times10^{-3}\,\mathrm{eV}^2$. Right: Contours in the plane of $\sin^2\theta_{13}$ and the flux normalization f. Colored regions (curves) correspond to Chooz + PV with (without) including the SBL experiments.

We show the $\Delta\chi^2$ from the Chooz and Palo Verde experiments as a function of $\sin^2\theta_{13}$ in Fig. 6 (left) for various assumptions on the fluxes. If the new fluxes are taken at face value and SBL reactor experiments are not included in the fit (solid green curve), we obtain from Chooz and Palo Verde a hint for $\theta_{13} > 0$ at about 90% CL, with a best fit value at $\sin^2\theta_{13} = 0.021$. In this case $\bar{\nu}_e$ disappearance due to θ_{13} accounts for the suppression of the observed rate at $L \simeq 1$ km relative to the slightly increased prediction from the new fluxes. However, as soon as SBL reactor experiments are included in the fit, the hint essentially disappears and $\theta_{13} = 0$ is consistent within 1σ. This can be understood from Fig. 5, which shows that the SBL reactor experiments pull down the flux predictions, leaving less room for a suppression at 1 km due to θ_{13}. The upper limit on $\sin^2\theta_{13}$ is very similar with old and new fluxes when SBL data are included, irrespective of whether the normalization is left free or not. These results are in agreement with Ref. [6]. Fig. 6 (right) shows the correlation between $\sin^2\theta_{13}$ and the flux normalization f with and without SBL experiments.

To summarize this section we emphasize that due to the tension between the new flux predictions and the short baseline oscillation data, including or not the SBL reactors in the fit leads to different results concerning the extracted value of θ_{13}. This will indeed be seen in our subsequent fit results, see for example, Sec. 5.

4. Solar + KamLAND analysis in the light of new reactor fluxes

The release of new solar data from the second and third phase of the Super-Kamiokande [10, 11] experiment, new data from the reactor experiment KamLAND [13],

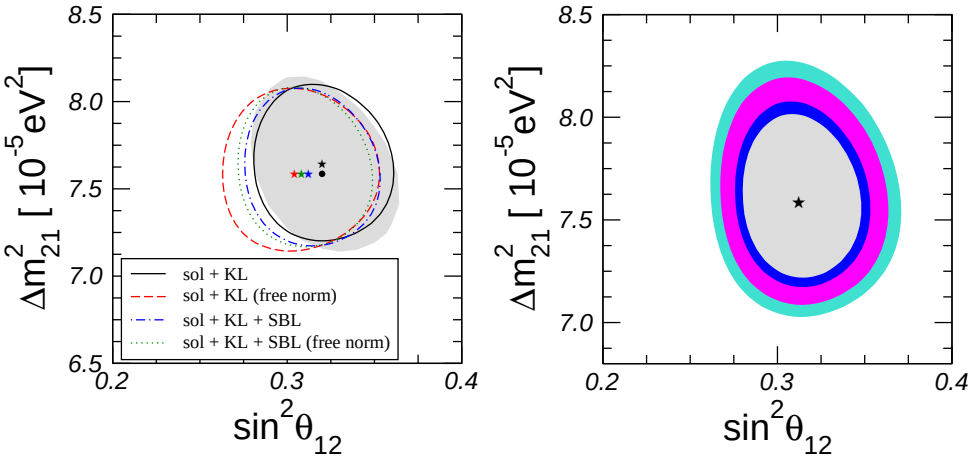

Figure 7. Left: 2σ allowed regions in the $\sin^2\theta_{12} - \Delta m^2_{21}$ plane from the analysis of solar + KamLAND data minimizing over θ_{13}. The different curves show the results obtained using different assumptions for reactor data, as indicated in the legend. For comparison we show as grey-shaded area the region obtained in our previous solar + KamLAND data analysis. Right: region allowed at 90%, 95%, 99%, 99.73% CL in our recommended analysis of solar + KamLAND data including SBL reactor results.

and the new predictions for the reactor anti-neutrino fluxes require a full revision of the solar + KamLAND neutrino data analysis. In Fig. 7 we show the 2σ allowed region from the solar + KamLAND neutrino data using different assumptions in the reactor data analysis, such as including or not including the short-baseline data or the use of a free normalization factor for the reactor anti-neutrino fluxes. In all cases the shift of the allowed region is not very significant, and the best fit point values vary between 0.304 and 0.320 for $\sin^2\theta_{12}$ while the solar mass splitting Δm^2_{21} goes from 7.59 to 7.64×10^{-5} eV^2. The variation in $\sin^2\theta_{12}$ is a bit larger because this parameter is correlated with the shift on $\sin^2\theta_{13}$, as shown in Fig. 8.

In the left panel of Fig. 8 we show the 2σ allowed regions in the $\sin^2\theta_{12} - \sin^2\theta_{13}$ plane for different choices of the reactor data analysis. For comparison we also show in grey the 2σ allowed region obtained from solar data only. In the right panel of Fig. 8 we show the constraints on θ_{13} from the combination of solar and KamLAND data. For the global neutrino oscillation fit presented in the following we will use the analysis of KamLAND + SBL data without free normalization, labelled as "sol+KL+SBL" in Fig. 8. In this case we get the following best fit value for θ_{13}:

$$\sin^2\theta_{13} = 0.023^{+0.016}_{-0.013} \quad \text{(solar + KamLAND)} \tag{3}$$

with $\Delta\chi^2(\sin^2\theta_{13} = 0) = 2.9$, and therefore a 1.7σ hint for $\theta_{13} \neq 0$ coming from the solar sector. Comparing with our previous analysis [1], the inclusion of new solar and KamLAND data and the new reactor fluxes results in a similar best fit value for the θ_{13} mixing angle (before we got $\sin^2\theta_{13} = 0.022$), but a slightly larger significance for non-zero θ_{13} (before: $\Delta\chi^2$= 2.2). The origin for this is mainly the preference of KamLAND data for a non-zero θ_{13} visible in the left panel of Fig. 8. For KamLAND θ_{13} acts mainly

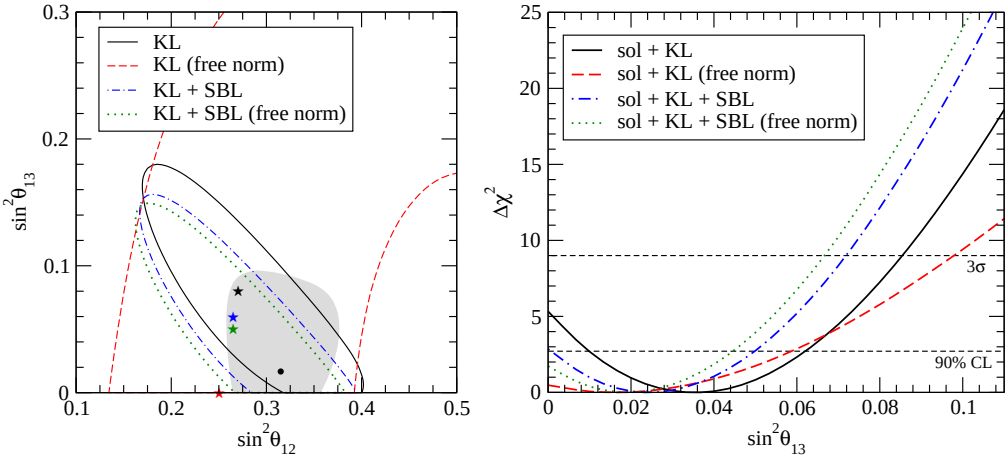

Figure 8. Left: 2σ allowed region in the $\sin^2\theta_{12} - \sin^2\theta_{13}$ plane obtained from KamLAND data using different assumptions on the reactor data analysis. For comparison we also show the 2 σ allowed region from solar data only (grey-shaded area). Right: $\Delta\chi^2$ as a function of $\sin^2\theta_{13}$ for the solar + KamLAND data analysis under the same assumptions as in the left panel.

as an overall reduction of the spectrum, and therefore the increased event rate due to the new reactor fluxes can be compensated by a non-zero θ_{13} in KamLAND.

Let us mention that Ref. [6] also investigates the implication for θ_{13} of reactor neutrino data in the light of the new fluxes. Our results are in reasonable agreement, although minor quantitative differences occur presumably due to different data used as well as different analysis strategies.

5. Global 3-neutrino analysis and status of θ_{13}

Let us now present the results of the global analysis combining all data mentioned in the previous sections ‖. As default for the reactor analysis we use the new anti-neutrino flux predictions and include in the analysis the SBL reactor experiments as discussed in Sec. 3.

Fig. 9 shows the χ^2 profile as a function of $\sin^2\theta_{13}$ for various data samples. In the upper part of Table 1 we display the corresponding best fit values and the significance for $\theta_{13} > 0$. In our standard recommended analysis (new reactor fluxes, SBL reactors included) we find no significant hint from Chooz and Palo Verde data, but the 1.7σ hint from solar + KamLAND (see Sec. 4) and the 1.3σ (1.4σ for IH) hint from atmospheric + MINOS data (see Sec. 2.3) combine to a global hint at 1.8σ for NH and IH, to be compared with the 1.5σ obtained in our previous analysis. In the lower part of Table 1 we discuss how this result depends on details of the reactor neutrino analysis. If SBL data are not used in the fit the significance for $\theta_{13} > 0$ is pushed close to 3σ because as discussed in Sec. 3 in this case also Chooz and Palo Verde prefer $\theta_{13} > 0$ at about 90% CL. However, in the flux-free reactor analysis as well as with the old reactor

‖ See also Refs. [1, 2] for previous experimental references.

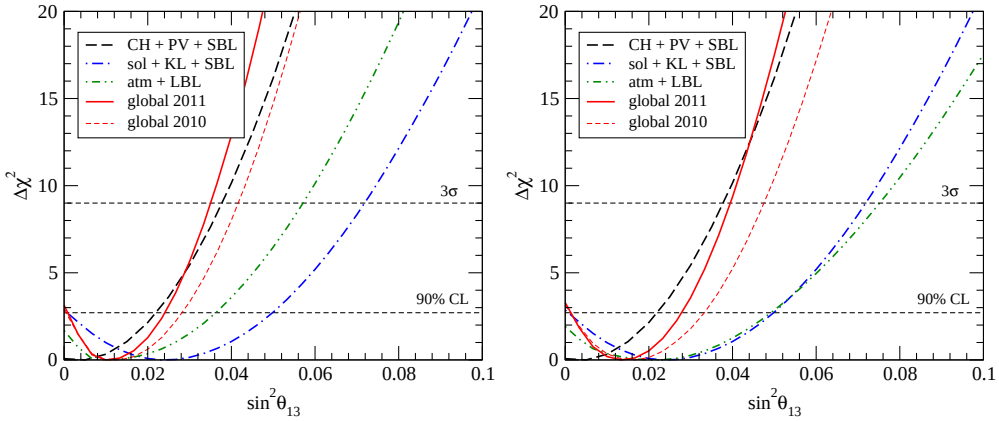

Figure 9. Constraint on $\sin^2\theta_{13}$ from different data sets, shown for NH (left) and IH (right). The curves labeled "CH+PV+SBL" include the Chooz, Palo Verde and the short-baseline reactor experiments, "solar+KL+SBL" include solar, KamLAND and short-baseline reactor data, and "atm + LBL" include Super-K atmospheric data, MINOS (disappearance and appearance), and K2K. The results from our previous 2010 analysis are also shown for comparison.

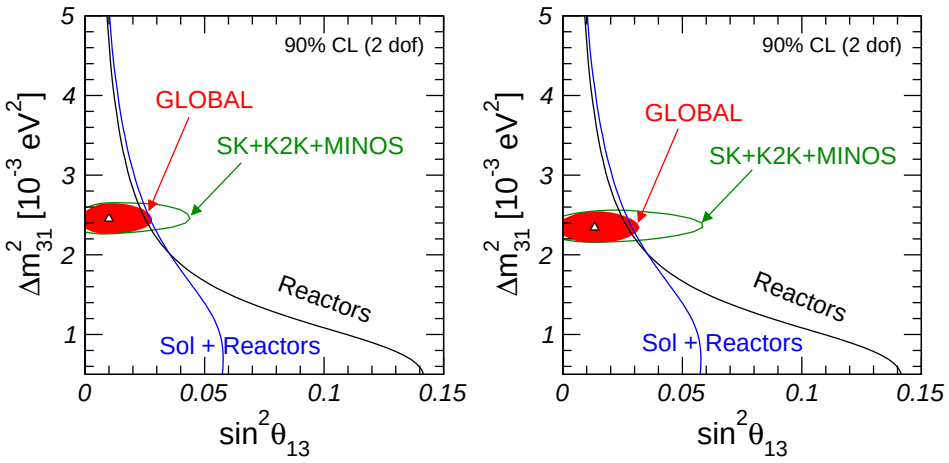

Figure 10. Illustration of the interplay of the global data on the $\sin^2\theta_{13}$ bound. Left: NH and right: IH.

fluxes the hint decreases to about 1.4σ and 1.8σ, respectively. The entry in the table labeled "global without reactors" comes from atmospheric and solar neutrinos plus data from the MINOS long-baseline experiment. Therefore, these results are independent of any ambiguity due to reactor fluxes, and we observe that a non-trivial limit on θ_{13} emerges even in this case. Let us mention that here we always assume the AGSS09 solar model [30]. As discussed previously [1, 3] there is a minor dependence of the hint for θ_{13} on this assumption.

Fig. 10 illustrates the interplay of the various data sets in the plane of $\sin^2\theta_{13}$ and Δm^2_{31}. In Table 2 we summarize the determination of neutrino oscillation parameters for our reference default reactor analysis. As discussed in Sec. 4 the impact of this choice upon the leading oscillation parameters is small. We find that inverted hierarchy gives a

	$\sin^2\theta_{13}$	$\Delta\chi^2(\theta_{13}=0)$	3σ bound
solar + KamLAND + SBL	$0.023^{+0.016}_{-0.013}$	2.9 (1.7σ)	0.072
Chooz + Palo Verde + SBL	$0.005^{+0.010}_{-0.020}$	0.07 (0.26σ)	0.038
atmospheric + MINOS	$0.010^{+0.016}_{-0.008}$	1.7 (1.3σ)	0.057
	$0.020^{+0.018}_{-0.015}$	1.9 (1.4σ)	0.075
global without reactors	$0.013^{+0.014}_{-0.009}$	2.3 (1.5σ)	0.053
	$0.020^{+0.015}_{-0.012}$	2.7 (1.6σ)	0.065
global with SBL	$0.010^{+0.009}_{-0.006}$	3.1 (1.8σ)	0.035
	$0.013^{+0.009}_{-0.007}$	3.3 (1.8σ)	0.039
global with SBL (free norm)	$0.007^{+0.009}_{-0.005}$	2.0 (1.4σ)	0.032
	$0.010^{+0.009}_{-0.007}$	1.9 (1.4σ)	0.037
global without SBL	$0.020^{+0.010}_{-0.008}$	7.0 (2.6σ)	0.048
	$0.027^{+0.009}_{-0.010}$	8.0 (2.8σ)	0.054
global without SBL (old fluxes)	$0.012^{+0.010}_{-0.007}$	2.9 (1.7σ)	0.042
	0.017 ± 0.010	3.2 (1.8σ)	0.048

Table 1. The best fit values for $\sin^2\theta_{13}$ with 1σ errors, the significance of the $\theta_{13} > 0$ hint, and the upper bound on $\sin^2\theta_{13}$ at 3σ for different data samples and for different reactor neutrino data assumptions. For a given global analysis the upper (lower) numbers refer to normal (inverted) neutrino mass hierarchy. We always use the new reactor fluxes [5] except for the row labeled "old fluxes" which uses previous results [19]. The row labeled "free norm" assumes a free reactor anti-neutrino flux normalization.

parameter	best fit $\pm 1\sigma$	2σ	3σ
Δm^2_{21} [10^{-5}eV^2]	$7.59^{+0.20}_{-0.18}$	7.24–7.99	7.09–8.19
Δm^2_{31} [10^{-3}eV^2]	2.45 ± 0.09	$2.28 - 2.64$	$2.18 - 2.73$
	$-(2.34^{+0.10}_{-0.09})$	$-(2.17 - 2.54)$	$-(2.08 - 2.64)$
$\sin^2\theta_{12}$	$0.312^{+0.017}_{-0.015}$	0.28–0.35	0.27–0.36
$\sin^2\theta_{23}$	0.51 ± 0.06	0.41–0.61	0.39–0.64
	0.52 ± 0.06	0.42–0.61	
$\sin^2\theta_{13}$	$0.010^{+0.009}_{-0.006}$	≤ 0.027	≤ 0.035
	$0.013^{+0.009}_{-0.007}$	≤ 0.031	≤ 0.039

Table 2. Neutrino oscillation parameters summary. For Δm^2_{31}, $\sin^2\theta_{23}$, and $\sin^2\theta_{13}$ the upper (lower) row corresponds to normal (inverted) neutrino mass hierarchy. We assume the new reactor anti-neutrino fluxes [5] and include short-baseline reactor neutrino experiments in the fit.

slightly better fit, however, with only $\Delta\chi^2 = 0.54$ with respect to the best fit in normal hierarchy.

6. Summary and conclusions

We have presented an updated global fit to world's neutrino oscillation data. The recent re-evaluation of the anti-neutrino fluxes emitted in nuclear power plants [5] introduces some ambiguity in the results obtained for the mixing angle θ_{13}. Since the new predictions are in slight disagreement with data from short-baseline (SBL) reactor experiments, with $L \lesssim 100$ m, it becomes necessary to include these data in the fit. A flux-free analysis of SBL data prefers an off-set of the reactor neutrino flux of about 6% from the predicted value with a significance of about 2.5σ. Taken at face value this might indicate either some un-accounted systematic effect (either in the new calculations or in the reactor data), or even the presence of some kind of new physics such as sterile neutrino oscillations with $\Delta m^2 \sim 1$ eV^2 [6]. Here we stick to the three-flavour framework, the sterile neutrino hypothesis will be discussed elsewhere [31].

Despite this hint for a deviation of the observed reactor anti-neutrino flux from its prediction, the goodness-of-fit of the SBL reactor neutrino data with the new fluxes is still very good ($\chi^2 = 13$ for 12 degrees of freedom). Motivated by this result, we adopt as our recommended default analysis the new fluxes and include the SBL data in the fit. In such a way we obtain a hint for $\theta_{13} > 0$ at 1.8σ, coming from a preference for a finite θ_{13} from KamLAND data combined with a somewhat weaker hint from the joint analysis of atmospheric + MINOS data. In Table 1 we show in detail how the global result depends on the assumptions on the reactor neutrino analysis, yielding hints for $\theta_{13} > 0$ ranging between 1.4σ and 2.8σ, with best fit values between $\sin^2\theta_{13} = 0.007$ and 0.027. This somewhat ambiguous situation regarding θ_{13} emerges from the slight tension due to the new reactor flux predictions with data. It will be interesting to see how the upcoming results from new reactor as well as accelerator experiments searching for θ_{13} will contribute to resolving the issue, see Ref. [18] for an overview and references.

The main results of our recommended default analysis of three-neutrino oscillation parameters are summarized in Table. 2 and in the right panels of Figs. 3 and 7 for the leading "atmospheric" and "solar" oscillation parameters, as well as in Fig. 10 for the mixing angle θ_{13}.

Acknowledgments

We thank Ed Kearns for discussions during Neutrino 2010 and, in particular, for providing us the Super-Kamiokande Collaboration χ^2 map obtained in Ref. [12]. We also thank T. Lasserre, M. Fechner and D. Lhuillier for communication on the SBL reactor analysis in relation to the new fluxes. Work supported by Spanish grants FPA2008-00319/FPA, MULTIDARK Consolider CSD2009-00064, PROMETEO/2009/091, and by EU network UNILHC, PITN-GA-2009-237920. M.T. acknowledges financial support from CSIC under the JAE-Doc programme. This work was partly supported by the Transregio Sonderforschungsbereich TR27 "Neutrinos and Beyond" der Deutschen Forschungsgemeinschaft.

References

[1] T. Schwetz, M. A. Tortola and J. W. F. Valle, New J. Phys. **10** (2008) 113011 [arXiv:0808.2016v3 [hep-ph]].

[2] M. Maltoni, T. Schwetz, M. A. Tortola and J. W. F. Valle, New J. Phys. **6** (2004) 122 [arXiv:hep-ph/0405172].

[3] M. C. Gonzalez-Garcia, M. Maltoni and J. Salvado, JHEP **1004** (2010) 056 [arXiv:1001.4524 [hep-ph]].

[4] Talk by E. Lisi at "Neutrino Telescopes", March 15–18, 2011, Venice, Italy, http://neutrino.pd.infn.it/Neutel2011/

[5] T. A. Mueller *et al.*, arXiv:1101.2663 [hep-ex].

[6] G. Mention *et al.*, 1101.2755 [hep-ex].

[7] P. Adamson *et al.* [The MINOS Collaboration], arXiv:1006.0996 [hep-ex].

[8] P. Vahle, [The MINOS Collaboration]. Talk at the Neutrino 2010 Conference, Athens, 2010.

[9] P. Adamson *et al.* [The MINOS Collaboration], arXiv:1103.0340 [hep-ex].

[10] J. P. Cravens *et al.* [Super-Kamiokande Collaboration], Phys. Rev. D **78**, 032002 (2008) [arXiv:0803.4312 [hep-ex]].

[11] K. Abe *et al.*, arXiv:1010.0118 [hep-ex].

[12] R. Wendell *et al.* [Super-Kamiokande Collaboration], Phys. Rev. D **81**, 092004 (2010) [arXiv:1002.3471 [hep-ex]].

[13] A. Gando *et al.*, arXiv:1009.4771 [hep-ex].

[14] Y. Takeuchi, [Super-Kamiokande Collaboration]. Talk at the Neutrino 2010 Conference, Athens, 2010.

[15] P. Huber, J. Kopp, M. Lindner, M. Rolinec and W. Winter, Comput. Phys. Commun. **177** (2007) 432 [arXiv:hep-ph/0701187].

[16] M. Maltoni and T. Schwetz, Phys. Rev. D **68** (2003) 033020 [arXiv:hep-ph/0304176].

[17] P. Adamson *et al.* [MINOS Collaboration], Phys. Rev. Lett. **103**, 261802 (2009) [arXiv:0909.4996 [hep-ex]].

[18] M. Mezzetto, T. Schwetz, J. Phys. G **G37** (2010) 103001. [arXiv:1003.5800 [hep-ph]].

[19] K. Schreckenbach, G. Colvin, W. Gelletly *et al.*, Phys. Lett. **B160** (1985) 325-330; A. A. Hahn, K. Schreckenbach, G. Colvin *et al.*, Phys. Lett. **B218** (1989) 365-368; F. Von Feilitzsch, A. A. Hahn, K. Schreckenbach, Phys. Lett. **B118** (1982) 162-166.

[20] P. Vogel, G. K. Schenter, F. M. Mann *et al.*, Phys. Rev. **C24** (1981) 1543-1553.

[21] Y. Declais *et al.*, Phys. Lett. B **338** (1994) 383.

[22] A. A. Kuvshinnikov *et al.*, JETP Lett. **54**, 253 (1991). [Sov. J. Nucl. Phys. **52**, 300 (1990)].

[23] Y. Declais *et al.*, Nucl. Phys. B **434** (1995) 503.

[24] G. S. Vidyakin *et al.*, Sov. Phys. JETP **66**, 243 (1987) [Zh. Eksp. Teor. Fiz. **93**, 424 (1987)]; JETP Lett. **59**, 390 (1994) [Pisma Zh. Eksp. Teor. Fiz. **59**, 364 (1994)].

[25] H. Kwon *et al.*, Phys. Rev. D **24** (1981) 1097.

[26] G. Zacek *et al.*, Phys. Rev. D **34**, 2621 (1986).

[27] M. Apollonio *et al.* [CHOOZ Collaboration], Eur. Phys. J. C **27**, 331 (2003) [arXiv:hep-ex/0301017].

[28] F. Boehm *et al.*, Phys. Rev. D **64**, 112001 (2001) [arXiv:hep-ex/0107009].

[29] M. Maltoni, T. Schwetz and J. W. F. Valle, Phys. Lett. B **518** (2001) 252 [arXiv:hep-ph/0107150].

[30] A. Serenelli, S. Basu, J. W. Ferguson and M. Asplund, arXiv:0909.2668 [astro-ph.SR].

[31] J. Kopp, M. Maltoni and T. Schwetz, arXiv:1103.4570 [hep-ph].